THE DESCRIPTION OF SHAPE DEVELOPMENT OF 2 DIMENSIONAL (SEMI)-ELLIPTIC SURFACE DEFECTS USING A MAXIMUM COMPLIANCE INCREASE HYPOTHESIS FOR DEFECT GROWTH

H. C. van Elst and J. W. Tichler

Department of Strength of Structural Materials, Metal Research Institute TNO, Apeldoorn, The Netherlands

ABSTRACT

Assuming that defect growth in general will aspire to occur in such a way that a maximum compliance increase is achieved, it proved possible to derive a 2d-crack extension law, which amply describes observed phenomena. It can be regarded as accounting for Paris relation-like descriptions, though it specifies the exponent in this relation as 2. Numerical calculations for 2d-semi elliptic surface defects confirmed a semi theoretical expression for the compliance as did experimental observations. The influence of crack extension on deformation was analysed and confirmed in view of its potential to follow crack growth.
Reliability assessments of structures, in particular design life prediction of off-shore components and vessels are thought to benefit from these crack growth considerations.

KEYWORDS

2-dimensional defect extension; compliance increase; embedded crack; surface crack; semi-elliptical defect; crack surface marking technique; varying load.

INTRODUCTION

For the reliability assessment of structural components the understanding of the extension of defects under service conditions (varying load, environmental circumstances involving corrosion, thermal fatigue, irradiation, etc.) appears of primary importance. Most of the analyses on crack growth pertain to "through crack" behaviour and can be considered based on the relation of Paris (1962) and its versions. Cf. e.g. Pelloux (1970); Forman, Kearney and Engle (1967) and Saxena, Hudak, Jouris (1979). However, cracks often develop as embedded or surface defects in a 2-dimensional way and the application of the current "through crack" extension description for this case has to be regarded with some reserve. In this paper the growth of (embedded and surface) cracks is investigated in a theoretical, numerical and experimental way, assuming on physical grounds that a maximum compliance increase will govern crack growth in a general way. This appears to offer a somewhat better consistency with experimental data than with the phenomenological relations (as of Paris) derived from "through crack" behaviour.

THEORETICAL

Embedded Defects

The extension of an elliptic 2d-defect embedded in a large ("infinite") solid under varying load transversal to the defect is considered. The extension in each point of its circumference normal to it, is then tangent to a hyperbole through this point, confocal to the initial ellipse. This suggests that the extended defect will remain elliptic by being confocal to the initial ellipse and its confocal hyperbolae as well. Indicating the minor axis by a 2a and the major axis by 2c, one will then have as a consequence of such behaviour:

$$c_o^2 - a_o^2 = c^2 - a^2 = d^2 = \text{constant or } \Delta a/\Delta c = c/a \qquad (1)$$

This is corroborated by the following more detailed analysis based on compliance considerations. According to Irwin (1962) the stress intensity factor along the circumference of the ellipse for a gross stress σ, corresponding with the applied load, reads:

$$K = \left[\sigma\sqrt{\pi a}\{\sin^2\phi + (a^2/c^2)\cos^2\phi\}^{\frac{1}{4}}\right]/\Phi$$

ϕ = polar angle of a point on the ellipse circumference with respect to the ellipse centre;

$$\Phi = \int_0^{\pi/2} \left[1-\{1-(c^2/a^2)\}\sin^2\phi\right]^{\frac{1}{2}} d\phi = \frac{\pi}{2}\left[1-\tfrac{1}{4}\frac{c^2-a^2}{c^2} - \frac{3}{64}\left(\frac{c^2-a^2}{c^2}\right)^2 \ldots\right] \simeq \frac{3\pi}{8} + \frac{\pi}{8}\frac{a^2}{c^2} \ldots \qquad (2a)$$

At the end of the minor axis: $\phi = \pi/2$; $K_{\phi=\pi/2} = \sigma\sqrt{\pi a}/\Phi$ (3a)

At the end of the major axis: $\phi = 0$; $K_{\phi=0} = \sigma\sqrt{\pi a^2/c}/\Phi$ (3b)

According to the Paris relation: $\Delta a = k(\Delta\sigma/\Phi)^m(\pi a)^{m/2}\,\Delta N$

$$\Delta c = k(\Delta\sigma/\Phi)^m(\pi a)^{m/2}\,(a/c)^{\frac{1}{2}}\,\Delta N$$

k and m are the well-known assumed "constants" in the Paris relation, N is number of applied load cycles.
Consequently:

$$\Delta a = (c/a)^{m/2}\,\Delta c \qquad (4)$$

(1) and (4) only appear compatible for m = 2.

Applying a plastic zone correction $r_p = K^2/4\pi\sqrt{2}Y^2$ (for a plastic constraint factor $\sqrt{2\sqrt{2}}$ (Irwin, 1960) and with Y = yield strength) to the physical crack dimension a, the stress intensity factor of the elastically treatable mathematical crack, becomes:

$$K = \frac{\sigma\sqrt{\pi a}}{\sqrt{\Phi^2 - \frac{1}{4\pi\sqrt{2}}\sigma^2/Y^2}}\{\sin^2\phi + (a^2/c^2)\cos^2\phi\}^{\frac{1}{4}} \qquad (2b)$$

not interfering with (4).
If only is assumed that the extended ellipse remains elliptic, (4) implies:
$c^n - a^n$ = constant, with n = m/2 + 1.
A possible description of defect extension might be based on the physical

principle, that the cause of extension will be optimally counter-balanced by its consequence; this inertia concept can be regarded inherent to the second law of thermo-dynamics. This would imply that extension takes place in such a way, that the increase in compliance C will be maximum.
Obviously, with f = CF (f = deflection; F = load):

$$F\,df = F^2\,dC + F\,C\,dF = dU + dW = C\,F\,dF + \tfrac{1}{2}F^2\,dC + G\,dA$$

with U = elastic potential energy; W = dissipated energy;
G = fracture resistance; dA = dπac = πadc + πcda = incremental fracture surface

Thus:

$$G = \tfrac{1}{2}F^2\,\frac{dC}{dA} \tag{6a}$$

With (1) this would read:

$$G = F^2\{c/2\pi(a^2 + c^2)\}\,\frac{dC}{da} \tag{6b}$$

Assume that the embedded crack is centrally located in the circular cross section with radius R of a cylinder with length L, loaded in axial direction and be:

$$\alpha \cong a/R < \gamma \equiv c/R << 1 \tag{7}$$

(6b) then reads:

$$G = \frac{F^2}{2\pi R^2}\,\frac{\gamma}{\alpha^2 + \gamma^2}\,\frac{dC}{d\alpha} \tag{6c}$$

It will be demonstrated that (6b), (6c) follows from (6a) applied to a circular defect by combination with the maximum compliance increase hypothesis for defect growth, i.e. (1) is then confirmed. For a circular embedded defect a = c = r and using r as index to refer to this situation:

$$K_r = \sigma\sqrt{\pi r}/\frac{\pi}{2} = 2\sigma\sqrt{\rho R}/\pi \quad \text{with} \quad \rho = r/R \quad ; \quad G_r = K_r^2\,(1-\nu^2)/E = 4\sigma^2\,\rho\,R\,(1-\nu^2)/\pi E$$

From (6c) with $\alpha = \gamma = r/R = \rho$

$$G_r = \frac{\sigma^2\,\pi\,R^2}{4\rho}\,\frac{dC_r}{d\rho}$$

$$\frac{dC_r}{d\rho} = \frac{16\rho^2\,(1-\nu^2)}{\pi^2\,E\,R} \quad ; \quad C_r - C_o = \frac{16\rho^3\,(1-\nu^2)}{3\pi^2\,E\,R} \quad \text{with} \quad C_o = \frac{L}{\pi\,R^2\,E} \tag{8a}$$

If $\Gamma \equiv C/C_o$ is the reduced compliance, the assumption of maximum compliance change at extension of an elliptic defect (α,γ) implies, that in the (α,γ,Γ)-space the displacement of $\Gamma(\alpha,\gamma)$ is in the gradient direction. For this gradient direction:

$$\frac{d\gamma}{d\alpha} = \frac{\partial\Gamma}{\partial\gamma}\Big/\frac{\partial\Gamma}{\partial\alpha} \tag{9}$$

while for a displacement along the Γ-surface, i.e. in tangential direction, one has:

$$d\Gamma = \frac{\partial\Gamma}{\partial\alpha} + \frac{\partial\Gamma}{\partial\gamma}\,\frac{d\gamma}{d\alpha} = 0 \quad \text{or} \quad \frac{d\gamma}{d\alpha} = -\frac{\partial\Gamma}{\partial\alpha}\Big/\frac{\partial\Gamma}{\partial\gamma},$$

this latter direction being orthogonal to (9).
$\Gamma(\alpha,\gamma)$ has to be symmetrical in α and γ. From (8a) with $\alpha = \gamma \doteq \rho$ one has

$$\Gamma_r = 1 + \lambda_r \rho^3 \text{ with } \lambda_r = \{16\ R\ (1-\nu^2)\}/3\pi\ L \tag{8b}$$

Generally for an embedded elliptic defect one can assume:

$$\Gamma(\alpha,\gamma) = 1 + \Psi(\alpha,\gamma), \text{ with } \Psi(\alpha,\gamma) = \Psi(\gamma,\alpha) = \Sigma\lambda_{ij}\alpha^{m_i}\gamma^{m_j} \tag{10a}$$

and $\lambda_{ij} = \lambda_{ji}$, while $m_k \neq 0$.
As from (8b) follows that for all i and j one has: $m_i + m_j = 3$, which is only compatible with $m_i = m_j = 3/2$, (10a) reads:

$$\Gamma(\alpha,\gamma) = 1 + \lambda\ \alpha^{3/2}\gamma^{3/2} \tag{10b}$$

As this implies: $\alpha \frac{\partial\Gamma}{\partial\alpha} = \gamma \frac{\partial\Gamma}{\partial\gamma} = 3/2(\Gamma-1)$

one concludes with (9):

$$\frac{d\gamma}{d\alpha} = \frac{\partial\Gamma}{\partial\gamma}\Big/\frac{\partial\Gamma}{\partial\alpha} = \frac{\alpha}{\gamma} \text{ or } \gamma^2 = \gamma_o^2 + \alpha^2 \tag{11}$$

According to (1) this proves that under the assumption that the defect extension is being governed by maximum compliance change and remaining elliptic, if being initially elliptic, the extension accordingly has to be along the normal direction in each point of the ellipse circumference, with the extended ellipse being confocal to the initial ellipse and its confocal hyperbolae, while m = 2 in (4).
The extension of an embedded elliptic defect will thus proceed in such a way, that an elliptic shape with the same foci remains retained. The experimental description for "through crack" extensions, with $m \neq 2$ need not be conflicting with the above made assumption, but rather suggests, that a correction factor Λ as required by geometry, material anisotropy, possibly environmental influence etc. has to be added, in the sense, that for a "through crack" with length b:

$$\frac{db}{dN} = k(\Delta K)^m \text{ is equivalent to } \frac{db}{dN} = k(\Delta K)^2\Lambda$$

by which also changes of m with "through crack" length might be accounted for.

Surface Defects

The extension of a half elliptic 2d-surface defect at the boundary surface of a large ("semi-infinite") solid under varying load transversal to the defect plane is considered next.
Due to the neighbourhood of the free surface containing the (major) axis 2c of the half elliptic defect, the stress intensity factor along the circumference requires a correction factor $M_e(\phi)$ to the expression (2a) or (2b).
Also again a plastic zone correction $r_p = K^2/4\pi\sqrt{2}Y^2$ (for a plastic constraint factor $\sqrt{2}\sqrt{2}$ and with Y = yield strength) might be added to physical crack dimensions to indicate the stress intensity factor; this does not interfere with the following.
Consider a prismatic specimen with rectangular cross section and sides w and 2v > w containing a half elliptic surface defect with half minor axis a//w and major axis 2c//2v.
Defining: $\alpha^* = a/w < \gamma^* \equiv c/w << 1$ (12)

the asterisks will be omitted for α and γ in the following in view of the similarity with the earlier definition (7) of α and γ, when analysing the embedded crack situation; otherwise for referring to the surface defect situation asterisks will be used. One will now have:

$$\Delta K^*_{\phi=\pi/2} = M_e(\tfrac{\pi}{2})\ \Delta\sigma\ (\pi a w)^{\frac{1}{2}}/\Phi \tag{13a}$$

$$\Delta K^{*}_{\phi=o} = M_e(0)\ \Delta\sigma\ (\pi\alpha w)^{\frac{1}{2}}/\Phi \qquad (13b)$$

Kobayashi and Moss (1969) indicate $M_e(\frac{\pi}{2}) = 1.03$ for the apex of the minor axis, independent of α for small α-values (here will be considered $\alpha < 0.5$).

For a half circular surface defect with a = c = r one has $dA = \pi w^2 \rho d\rho$, now with $\rho \equiv r/w$:

$$G_r^{*} = \frac{F^2}{2\pi w^2 \rho}\ \frac{dC_r^{*}}{d\rho} \qquad (14)$$

A reasonable assumption appears:

$$G_r^{*} = K_r^{*2}(1-\nu^2)/E = 4\bar{M}_{er}^{\ 2}\,\sigma^2 \rho w(1-\nu^2)/\pi E$$

with $\bar{M}_{er}$ = average M_e-value along the circumference of the half circular defect.

From (14):

$$\frac{dC_r^{*}}{d\rho} = 2\bar{M}_{er}^{\ 2}\rho^2 w\,(1-\nu^2)/Ev^2;\ \text{or}$$

$$C_r^{*} - C_o^{*} = 2\bar{M}_{er}^{\ 2}\rho^3 w\,(1-\nu^2)/3Ev^2 \text{ with } C_o^{*} = L/2vwE \qquad (15)$$

Introducing again: $\Gamma^{*} = C^{*}/C_o^{*}$

$$\Gamma_r^{*} = 1 + \frac{4}{3}\bar{M}_{er}^{\ 2}\rho^3\,(1-\nu^2)w^2/Lv = 1 + \lambda_r^{*}\rho^3 \qquad (16)$$

For a half elliptic surface defect one might again assume in analogy with (10a):

$$\Gamma^{*}(\alpha,\gamma) = 1 + \Sigma\,\lambda_{ij}^{*}\alpha^{m_i}\gamma^{m_j} \qquad (17)$$

with $m_i + m_j = 3$ and $\lambda_{ij}^{*} = \lambda_{ij}^{*}(\alpha,\gamma)$ taking account of $\bar{M}_e$, the average $M_e(\alpha,\gamma)$ for the half elliptic surface defect (α,γ) but now $\lambda_{ij}^{*} \neq \lambda_{ji}^{*}$ in view of the asymmetry of the surface defect situation as compared to the earlier considered embedded defect situation. From (10b) is readily suggested trying to retain again one term in (17) and to write accordingly:

$$\Gamma^{*}(\alpha,\gamma) = 1 + \lambda^{*}(\alpha,\gamma)\,\alpha^{3/2}\gamma^{3/2} \qquad (18)$$

Under NUMERICAL is elaborated that $\lambda^{*}(\alpha,\gamma) = \lambda_o^{*}\alpha^p\gamma^q$, with $\lambda_o^{*} = 0.78$; $p = 0.16^5$ and $q = 0.36$ offers a satisfactory approximation of $\Gamma^{*}(\alpha,\gamma)^o$ with (18). This implies as description for the half elliptic surface defect extension:

$$\frac{d\gamma}{d\alpha} = \frac{3/2 + q}{3/2 + p}\,\frac{\alpha}{\gamma} \text{ or } \gamma^2 = \gamma_o^2 + \frac{3/2 + q}{3/2 + p}\,\alpha^2 = \gamma_o^2 + \frac{1.86}{1.66^5}\,\alpha^2 = \gamma_o^2 + 1.12\,\alpha^2 \qquad (19)$$

NUMERICAL

Embedded Cracks

For an (experimental) specimen model as shown in Fig. 1 elastic compliance calculations were performed to verify the theoretically derived description (18). Translation of upper and lower surface was prescribed as boundary condition. The stresses will then vary with the location on these flat remaining surfaces,

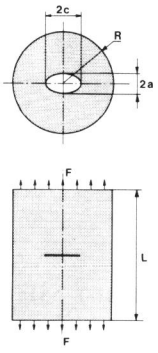

Fig. 1. Specimen model for embedded crack.

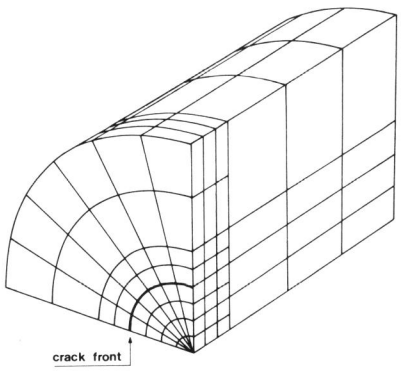

Fig. 2. Elements network for calculations on embedded cracks with *DIANA*.

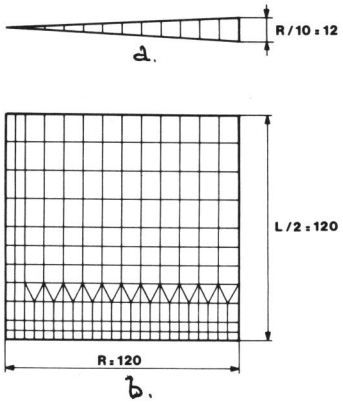

Fig. 3. Elements network for 2d-calculations on circular embedded cracks with *STARDYNE*.

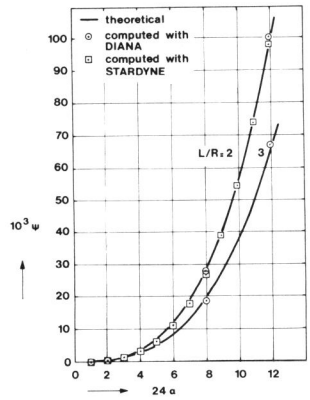

Fig. 4. Comparison of theory and results of calculations with programs *DIANA* and *STARDYNE* for circular defects.

obviously in a relative sense more, according to L/R being smaller. A restriction of these relative σ-variations was considered accomodating and L/R = 2 was investigated in this respect, taking R = 120 mm; ΔL = 2 mm; E = 200 x 10^3 N/mm^2; ν = 0.28.
For the circular embedded cracks 3d-calculations were performed with elements networks as shown in Fig. 2; the coordinates of the nodes were not varied at increase of the size of the circular defect.
Three-dimensional elastic calculations were performed for the elliptic embedded cracks with to the defect adapted elements networks, using the (by TNO developed) *DIANA* program. Moreover, as a comparison and control for the circular embedded cracks a distribution of small angle(ca. 6^o) cylinder sectors (Fig. 3a) was used to perform 2d-elastic calculations using the *STARDYNE* program with an elements network of the cylinder sectors as shown in Fig. 3b. The results of the presumably largest stress variations in the end faces for the largest considered $\alpha = \gamma$ value 0.5 for L/R = 2, showed a S.D. $\Delta\sigma$ in the average σ-value, amounting to 13%, which was considered unconveniently high (calculation 1, Table 1).
For L/R = 3 and $\alpha = \gamma = 0.5$ was found $\Delta\sigma/\bar{\sigma} = 2\%$.
Calculations 3 till 17, Table 1, give the $\Psi = \Gamma - 1$ values both with *STARDYNE* and *DIANA*. There exists a quite satisfactory agreement between the results of the application of both programs, as well as with the theory, reassuring the choice of the elements networks (cf. also Fig. 4), referring to circular defects.
Two- and three-dimensional *DIANA*-calculations (18 and 19 in Table 1) were compared for $\alpha = \gamma = 1/3$, showing the same results. Three-dimensional calculations for an embedded circular defect $\alpha = \gamma = 0.1667$ and an embedded elliptic defect $\alpha = 0.1333$, $\gamma = 0.2083$ (calculations 20 and 21 respectively in Table 1), presumably offering the same Ψ-value according to (18), showed a difference in Ψ of less than 5%, i.e. in Γ of less than 0,1%, illustrating the matching accuracy of the elastic *DIANA* calculations with the chosen elements networks for the elliptic and circular defect (cf. Fig. 2). There was 0.3% discrepancy in Γ-values according to theory and calculation.

Surface Defects

For an experimental specimen model as shown in Fig. 5 elastic compliance calculations were performed to verify the theoretically derived expression (18).
As boundary condition was now prescribed constant stress in upper and lower surface. The relative displacements ΔL/L will then vary with the location in these surfaces, the more according to L/R being smaller.
As numerical values were taken: w = 35 mm; 2v/w = 2; L/w = 3; σ = 200 N/mm^2; E = 200 x 10^3 N/mm^2; ν = 0.28.
All elastic calculations pertaining to surface defects were carried through in a 3-dimensional way, using the *DIANA* program for elements networks as shown in Fig. 6.
In Fig. 7 the α-γ values of the surface defects for which 3d-calculations were performed are represented in a α-γ diagram as the points: 2-8; 4-8; 6-8; 8-8; 4-10; 6-10; 8-10; 10-10; 6-12; 8-12; 10-12; 12-12; 12-14; 14-14; and 12-6, referring to 24α-24γ. The relevant calculations are indicated in Table 2 with the same 24α-24γ notation. In view of the lack of symmetry with these surface defects, as compared to embedded defects, now the results for 6-12 and 12-6 are presumably different. Obviously, only ¼ of the specimen model need to be considered, viz. as bounded by the symmetry plane, the cross section containing half of the semi-elliptic defect, half of the free surfaces and the end surface with the prescribed constant stress boundary condition. While for the constant displacement boundary conditions, used for analysing embedded cracks C = ΔL/F, one now has for the considered case of the surface defect, with F_i = nodal force in end face and thus $F = 2 \Sigma F_i$ = total load, for the totally performed work:

$$H = 4\Sigma H_i = 2\Sigma F_i f_i \text{ and } C = \Sigma F_i f_i / (\Sigma F_1)^2.$$

TABLE 1 Compliance calculations for embedded defects

Calculation	L/R	α	γ	10^3 ψ Theory	10^3 ψ *DIANA**	10^3 ψ *STARDYNE*	$\Delta\sigma/\bar{\sigma}$ *(DIANA)*
1	2	0.5000	=α	97.78	99.98	-	13%
2	3	0.5000	=α	65.19	66.85	-	2.2%
3	2	0.0417	=α	0.06	-	0.03	-
4	2	0.0833	=α	0.45	0.38	-	-
5	2	0.0833	=α	0.45	-	0.32	-
6	2	0.1250	=α	1.53	-	1.20	-
7	2	0.1667	=α	3.62	-	3.01	-
8	2	0.2083	=α	7.07	-	6.09	-
9	2	0.2500	=α	12.22	-	10.82	-
10	2	0.2917	=α	19.41	-	17.56	-
11	2	0.3333	=α	28.97	27.59	-	-
12	2	0.3333	=α	28.97	-	26.72	-
13	2	0.3750	=α	41.25	-	38.75	-
14	2	0.4167	=α	56.54	-	54.17	-
15	2	0.4583	=α	75.32	-	73.58	-
16(cf. 2)	2	0.5000	=α	97.78	-	97.70	-
17	3	0.0833	=α	0.30	0.25	-	-
18	3	0.3333	=α	19.32	18.42	-	-
19	3	0.3333	=α	19.32	18.40	-	-
20	3	0.1667	=α	2.41	2.14	-	-
21	3	0.1333	0.2083	2.41	2.05	-	-

* Calculations 1,2,4,11,17,18: 2d - *DIANA*; calculations 19,20,21: 3d - *DIANA*

TABLE 2 Comparison of calculated compliance of 2d-semi-elliptic surface defects with theoretical description (Cf. Fig. 8)

Elements network	Calculation	$10^3\Psi$	$10^3 \times 0.77\alpha^{1.7}\gamma^{1.8}$	x = 27.5; y = 0 ε in %	x = 27.5; y = 35 ε in %
1	8-8	17.3	16.5	0.1111	0.0930
	10-10	36.0	36.0	0.1224	0.0864
	12-12	67.5	68.1	0.1415	0.0768
	14-14	117.0	116.7	0.1713	0.0636
2	6-8	11.2	10.1	0.1076	0.0950
	8-10	25.5	24.6	0.1170	0.0894
	10-12	50.3	49.9	0.1334	0.0807
	12-14	90.8	89.8	0.1600	0.0683
3	4-8	5.6	5.1	0.1041	0.0971
	6-10	15.4	15.1	0.1113	0.0926
	8-12	34.1	34.1	0.1247	0.0852
4	2-8	1.4	1.4	0.1012	0.0992
	4-10	7.3	7.3	0.1059	0.0961
	6-12	20.2	20.2	0.1162	0.0903
	12-6	17.7	19.5	0.1094	0.0942

TABLE 3 Characterisation investigated Fe 510 steel plate with 70 mm thickness

Chemical analysis				Mechanical properties
C	0.18	Cu	0.019	yield strength; 380 N/mm^2
Mn	1.44	Su	0.006	ultimate tensile strength: 530 N/mm^2
P	0.016	W	0.039	A_5 (transversal r.d.) 30%
S	0.004	Ni	0.017	Z 28-62%
S	0.35	Nb	0.046	Charpy V value at -30°C 155 J

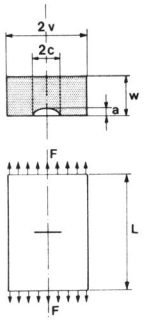

Fig. 5. Specimens model for surface defect.

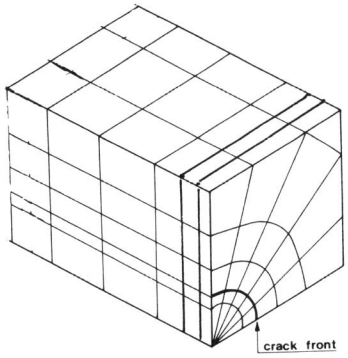

Fig. 6. Elements network for 3d-calculations on surface defects with *DIANA*.

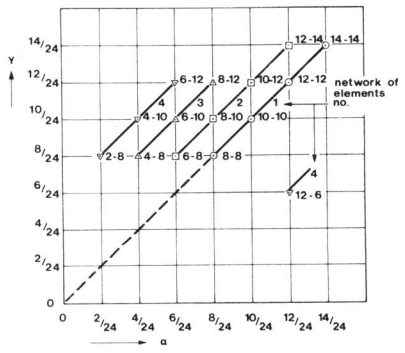

Fig. 7. Indication by α and γ values of surface defects for which 3d-calculations were performed.

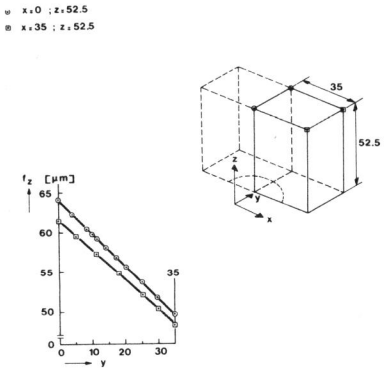

Fig. 8. Detail of calculation 12-12 revealing behaviour of displacement f_z.

The prescribed boundary condition implies absence of bending in the end surfaces. However, the defect containing cross section does contain a bending component. This implies a substantial gradient in the displacement on the end faces, which was analysed for the 12-12 surface defect. From details of the relevant calculation 12-12 it pursued that the displacements along the symmetry line and along the smaller boundary edge in the end surface present a linear decrease from front surface side (i.e. side where the surface crack is situated) to back surface side; the latter slightly larger (4 to 5%) than the former.
As displacement of the upper or lower surface can thus be taken the arithmetic mean of the displacements of its front and back layer boundary edge. Cf. the plot of Fig. 8.
The results of the compliance calculation are given in Table 2. The feasibility of a description of the obtained $\Psi = \Gamma - 1$ values by $\lambda^{*}\alpha^{3/2+p}\gamma^{3/2+q}$ was investigated using an **iteration** method (rather than a linear regression analysis of ln Ψ), with as results: $\lambda_o^{*} = 0.7820$; $p = 0.1646$; $q = 0.3600$ (and with a residual strength summ = 0.748, corresponding with a relative S.D. of $\Delta\Psi/\Psi = 2.17\%$). In Table 2 the values of Ψ with $\lambda_o^{*} = 0.78$; $p = 0.16^5$ and $q = 0.36$ are given in comparison with the calculated values, illustrating a satisfying aptitude for description.

EXPERIMENTAL

Material

A normalized C-Mn steel, according to Euronorm **Fe510**, obtained from a Dutch steel firm as plate material with 70 mm thickness, was used for investigation of the 2-dimensional defect extension. Relevant properties are given in Table 3.
The constants in the Paris relation of this steel are given by Bristoll and Opdam (1978) as $k = 1.48 \times 10^{-12}$ and $m = 2.71$, (for N and mm units), while Overbeeke (1979) indicates $k = 6.1 \times 10^{-12}$ and $m = 3.0$. This material was chosen as it was also used in an ECSC-sponsored program on corrosion fatigue of off-shore structural material which involved TNO-activities and can be considered representative for application to present off-shore structures.

Preparation of Specimens with Defects

Embedded defects. Two half circle cylinder parts, obtained by cutting a full circle cylinder by a meridional plane through the axis, were provided with surface defects in the flat meridional surfaces transversal to the axis. (Cf. below under surface defects). The two half cylinders were than connected by a joint, showing in best approximation the same mechanical properties, as the specimen material.
Electron beam welding and high temperature soldering were explored as to their joining capacities. The former appeared to offer less guarantee for retaining the induced defect shape and consequently the latter was applied. The temperature had to remain below 880°C in order to avoid change in mechanical properties of the steel. Using vacuum soldering it proved possible to prevent filling of the defect by the soldering material.
Solder foils SCP_1, SCP_2 and SCP_3, with melting regions 807-810°C, 824-852°C and 850-900°C respectively and with 0.05 mm thickness were used; soldering temperatures were 875-850°C. Flow of the solder was quite good, reasonable and moderate for these foils respectively. Simulated cracks of 0.4 mm width and filled with anti-flow (green stop-off) proved absence of solder afterwards. The mechanical strength was 500-545 MN/m^2 for all solder types, as anticipated. The thickness of soldered joints of 30 mm slabs was 2-20 µm, being considerably less than the **50 µm** foil thickness, probably due to the weight of a slab pressing away the liquid solder
Regretfully experiments with embedded cracks obtained by soldering had to be cancelled, as sponsoring parties concluded that relevant calculations, as mentioned under NUMERICAL, were sufficiently conclusive.

Surface defects. The preparation of the surface defects proceeded by spark erosion. The largest part was realized with a 0.4 mm thickness electrode; for the last half mm a 0.2 mm thickness special electrode was used, providing the half elliptic circumference of the crack front. Three tensile specimens were prepared with gage-length 105 mm, width 68 mm, thickness 34 mm, initial defect dimensions corresponding with α = 4/24 and γ = 8/24, 9/24 and 10/24 resp. in the center of the width side. The dimensions of the enlarged ends of the tensile specimens were chosen as shown in Fig. 9 to allow use of available grips for the applied 2500 kN loading machine.

Investigation as to Suitable Marking Techniques of the Extending Crack Front on Bend Specimens

The defect extension experiments required a reliable crack front marking technique not interfering with the extension velocity. As such were investigated decrease during some load cycles of one of the parameters ΔK, $R = \sigma_{min}/\sigma_{max}$ and ν = loading frequency, respectively, keeping the others constant.
Moreover, etching of the crack surface during some cycles with "nital" (a 2 vol.% nitric acid solution in 96 vol.% alcohol) followed by cleaning with 96 vol.% alcohol during some cycles was applied. 6 single edge notched bend specimens were investigated as to the best marking method of the mentioned four. Loading was in the rolling direction and crack extension in the original plate thickness direction (i.e. according to ASTM-convention LS). Decrease of ΔK or R, keeping R,ν and K,ν constant respectively was not expected to have any influence on the defect extension velocity after this marking procedure.
Decrease of ν, keeping ΔK and R constant - and similarly of etching with "nital", which implied a frequency decrease as well for reasons of application - were investigated as to such an influence.
Striation measurements on **electron microscopic observations of the crack** surface after open breaking of the specimens submitted to varying load revealed significant larger striations at lower frequency, but no significant differences between striations before and after the marking procedure, involving frequency decrease.
The experiments were performed in steps, each step being realized with a certain load change ΔF corresponding with ΔK = 20-25 MPa $m^{\frac{1}{2}}$; midway each step a number of cycles was used for marking the crack front.
All steps were performed with R = 0.5 like the also performed surface crack extension experiments on tensile specimen reported below. Before the first step of these experiments on bend specimen an opposite bending load was applied during 30000 cycles with an amplitude equal to the intended bending load during the first step in order to facilitate crack initiation.
Experiment 1 was performed at 7 Hz (being the maximum frequency allowed by the for this experiment available loading equipment). Experiment 2 till 5 were performed at 20 Hz (on a larger capacity loading machine). In view of the frequency to be applied for tensile specimens (see below), experiment 6 was performed at 10 Hz. All the laboratory experiments on bend specimens were carried out at ambient temperature in air.

The open broken specimens were etched with "nital", which improved the observation of the markings. The step transitions, usually accompanied by a ΔK-decrease till 80% of the preceeding step were amply visible.
The ΔK-decrease meant for crack front marking showed a rather poor observation quality, which might be due to the relatively small number of marking cycles.
For specimen 6 the number of marking cycles was chosen in such a way, that an extension of the crack front of ca. 0.1 to 0.2 mm would take place (using for this estimate the data from Bristolland Opdam, loc.cit.).
It could be concluded that a frequency decrease till 0.5 Hz, during a number of cycles providing 0.1 mm further crack growth, offered good recording possibilities.

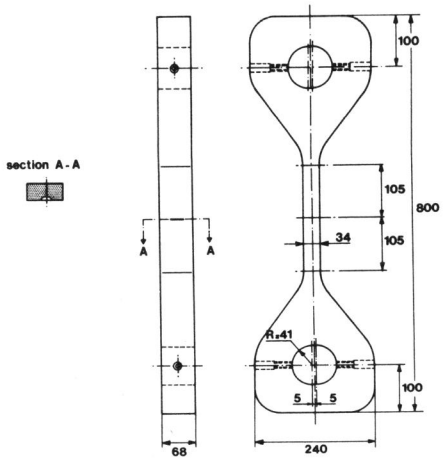

Fig. 9. Tensile specimen with surface defect.

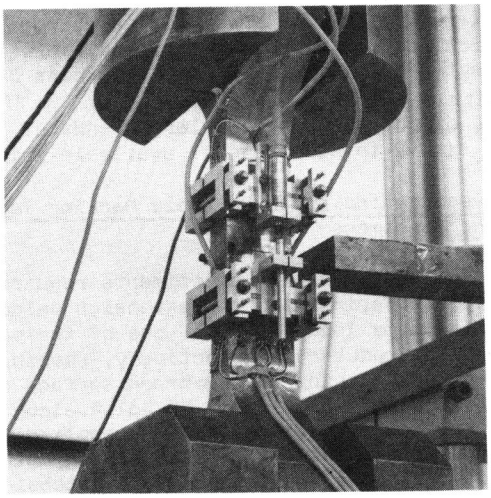

Fig. 10. Location of inductive displacement recorders and strain-gauges on tensile specimen.

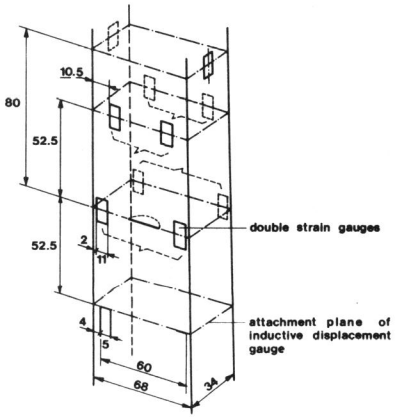

Fig. 11. Location of straingauges on tensile specimen.

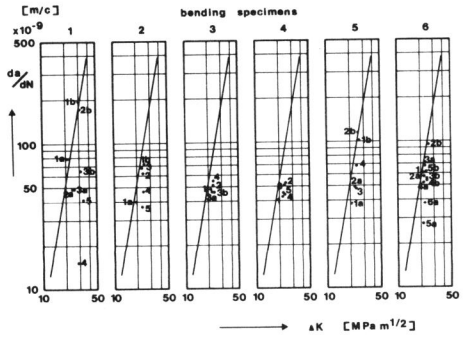

Fig. 12. Comparison of results of crack extension rate measurements of through-cracks in bend specimen with results of Bristol and Opdam, loc. cit.

Observation of Surface Defect Extension in Tensile Specimen

Pinloading of the tensile specimens was applied to avoid bending (cf. Fig. 9). Compliance measurements were performed using 2 electromagnetic inductive displacement gauges, viz. at the side, where the defect is located and at the opposite side on equal distances from the crack surface (cf. Fig. 10). For a gauge length of 105 mm the arithmetic means of the displacements as recorded by these gauges gave the compliance (cf. Fig. 8 and its corresponding conclusion in the text under NUMERICAL).
Straingauges were applied, as shown in Fig. 11. These were used in a double fashion and were arranged self correcting for temperature variations (the temperature coefficient of these straingauges being presumably quite comparable). The responses of strain gauge pairs on the same distance from the crack surface at both width sides were added and read. This also allowed at (the beginning of) each step to eliminate bending in two directions within 2%. Loading was again in the rolling direction with the minor axis of the semi-elliptic defects in the width direction of the original plate (ASTM convention LT). To restrict crack closure effects R = 0.5 was retained. Each step of the again stepwise performed experiment was carried out with constant minimum and maximum load, chosen such that an average ΔK = 20 MPa $m^{\frac{1}{2}}$ could be expected at the apex of the minor axis. The loading frequency was 5 Hz.
At the beginning of each test the specimen was submitted to 20000 cycles with a compressive load of 50% of the intended tensile load variation in the first step, in order to facilitate crack initiation. From a buckling analysis it was concluded that this was the highest tolerable compressive load. The first step of each test was interpreted as crack initiation ("pre cracking") and not used in the evaluation of the results. At the end of each step, crack front marking was induced by the decrease of frequency to 0.5 Hz.
These laboratory experiments on tensile specimens with a semi-elliptic surface defect were again carried out at ambient temperature in air. "Nital" was again used for etching the open broken specimens to improve the observation of the markings.

RESULTS

Through Crack Extension of Bend Specimens

Crack extension as a function of number of load cycles could be found from crack length measurements on open broken bend specimens. Results are presented in Table 4 and plotted in Fig. 12.
The obtained da/dN values are slightly below those communicated by Bristoll and Opdam, loc.cit.
The relative large discrepancy shown by the results of test 1 might have been caused by the rather poor load evaluation reliability of the used tensile equipment, that was available.

Crack Shape Developments of Semi-elliptic Surface Defects in Tensile Specimens

The results for tests 1, 2 and 3 are presented in Table 5. The a and c values were measured using the "open break" method for the specimen. Figs. 13a & 13b show the markings for extension of the defect in a bend and tensile specimen, respectively, after "open breaking"; Fig. 14 is an electron microscope image of the fracture appearance revealing striations as discussed under EXPERIMENTAL. c-values were measured in the two directions from the surface defect centre. The largest difference in these values was 1 mm in tensile specimen 2; this is less than 5% of the total c-value. In the other cases the asymmetry in the surface crack extension was less, usually even

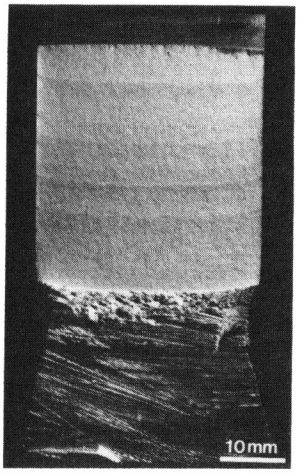

Fig. 13a. Crack surface appearance after open breaking of bend specimen.

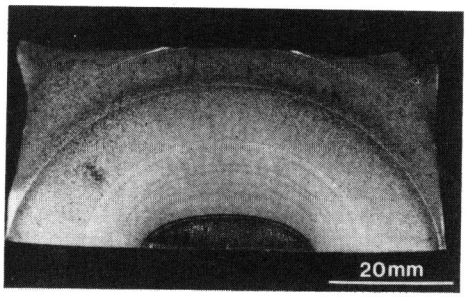

Fig. 13b. Crack surface appearance after open breaking of tensile specimen.

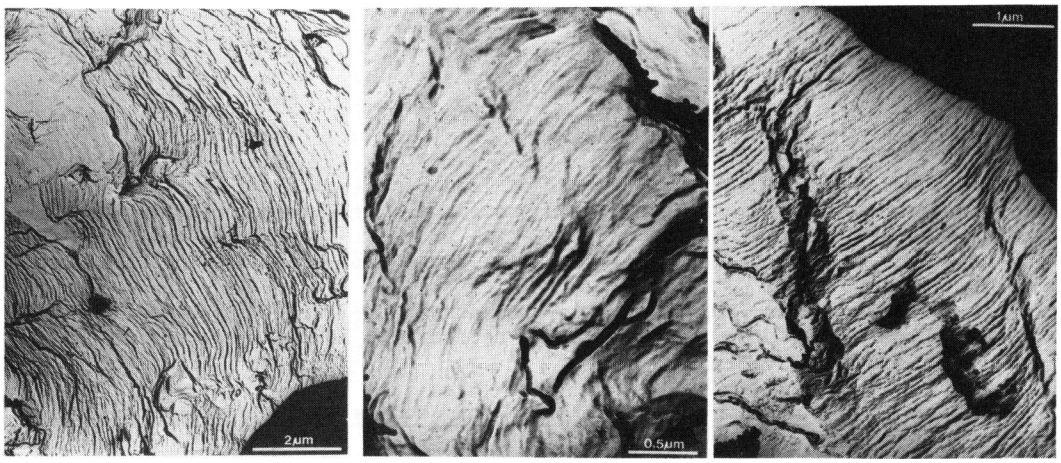

a. b. c.

Fig. 14. Electron microscopic fractograph, showing striations due to varying load cycles before (a), at (b) and after (c) marking.

TABLE 4 Crack growth observations on bend specimens

	Step	ΔF (kN)	a_1 (mm)	a_2 (mm)	$\bar{a}$ (mm)	ΔK (MPam$^{\frac{1}{2}}$)	Δa (mm)	ΔN (cycles)	Δa/ΔN (nm/cycle)
Spec.1	1a	60	4.3	11.1	7.1	21.6	6.9	88000	78
	1b	60	11.1	16.8	13.7	29.9	5.7	30000	189
	2a	40	16.8	23.0	19.7	25.1	6.2	127600	49
	2b	40	23.0	27.3	25.1	30.6	4.3	258000	167
	3a	27.5	27.3	32.4	29.8	25.3	5.1	104200	49
	3b	27.5	32.4	36.6	34.4	30.8	4.2	64500	65
	4	21	36.6	39.7	38.1	28.0	3.1	205200	15
	5	18	39.7	49.8	44.5	33.8	10.1	241900	42
Spec.2	1a	60	4.1	8.0	5.8	19.7	3.9	97800	40
	1b	60	8.0	11.5	9.6	24.9	3.5	48200	73
	2	47	11.5	17.0	14.0	23.8	5.5	89000	62
	3	38	17.0	22.1	19.4	23.6	5.1	76300	67
	4	32	22.1	26.6	24.3	23.9	4.5	95400	47
	5	26	26.6	31.3	28.9	22.9	4.7	128000	36
Spec.3	1	60	4.4	11.1	7.1	21.5	6.7	140300	48
	2	47	11.1	16.6	13.6	23.2	5.5	108500	51
	3a	38	16.6	21.3	18.8	22.9	4.7	101500	46
	3b	32	21.3	26.3	23.7	23.0	5.0	107800	46
	4	26	26.3	34.5	29.1	23.2	7.8	141600	55
Spec.4	1	60	4.6	11.7	7.5	22.3	7.1	164900	43
	2	47	11.7	16.8	14.1	23.8	5.1	95000	54
	3	38	16.8	21.7	19.1	23.3	4.9	94000	52
	4	32	21.7	26.5	24.0	23.5	4.8	108600	44
	5	26	26.5	32.0	29.1	23.2	5.5	121800	45
Spec.5	1a	60	4.4	8.8	6.3	20.5	4.4	116000	38
	1b	60	8.8	12.0	10.3	25.7	3.2	30900	104
	2a	47	12.0	15.2	13.5	23.1	3.2	64100	50
	2b	47	15.2	18.0	16.6	26.2	2.8	23900	117
	3	38	18.0	22.1	20.0	24.1	4.1	64800	48
	4	34.2	22.1	25.0	23.5	24.7	2.9	42200	69
Spec.6	1	60	4.9	10.5	7.3	21.6	5.6	91800	61
	2a	47	10.5	14.3	12.3	22.1	3.8	65000	58
	2b	47	14.3	16.9	15.5	25.1	2.6	27150	96
	3a	38	16.9	19.7	18.2	22.5	2.8	42360	66
	3b	38	19.7	20.9	20.3	24.3	1.2	21950	55
	4a	32	20.9	23.7	22.3	22.0	2.8	53420	52
	4b	32	23.7	26.1	24.9	24.2	2.4	44270	54
	5a	26	26.1	28.7	27.4	21.6	2.6	92720	28
	5b	26	28.7	31.0	29.8	23.7	2.3	37000	62
	6a	22	31.0	33.6	32.3	22.3	2.6	70530	37

a_1 = crack length in core of specimen at the beginning of a series of load cycles.

a_2 = crack length in core of specimen at the end of such a step of load cycles.

$\bar{a} = \{p\Delta a/(a_1^{-p} - a_2^{-p})\}^{1/(p+1)}$ with $p = m/2 - 1$ and $m = 2.71$; $\frac{da}{dN} = ka^{m/2}$;

$k\Delta N = (a_1^{-p} - a_2^{-p})/p$; $\frac{\Delta a}{\Delta N} = ka^{-m/2}$; $\bar{a} = (\Delta a/k\Delta N)^{1/(p+1)}$; $\Delta K = (S\Delta F/Bw^{3/2})/f(a/w)$;

$f(a/w) = 2.9(a/w)^{\frac{1}{2}} - 4.61(a/w)^{3/2} + 21.8(a/w)^{5/2} - 37.7(a/w)^{7/2} + 38.7(a/w)^{9/2}$. (S≡span)

TABLE 5 Semi-elliptical surface defect growth in tensile specimens.

	Step nr.	ν (Hz)	N (cycles)	$\bar{F}$ (kN)	ΔF (kN)	a (mm)	c (mm)
Tensile specimen 1	0	-	-	-	-	5.6	11.3
w = 34.0 mm	1	5	55420	540	360		
2v = 68.0 mm	Mark.	0.5	2160	540	360	8.2	12.6
	2	5	37960	486	324		
	Mark.	0.5	2160	486	324	10.0	13.6
	3	5	22950	465	310		
	Mark.	0.5	2500	465	310	11.4	14.6
	4	5	27000	465	310		
	Mark.	0.5	2900	465	310	13.5	16.5
	5	5	17340	447	298		
	-	-	-	-	-	15.1	18.0
Tensile specimen 2	0	-	-	-	-	5.6	14.1
w = 33.6 mm	1	5	38270	484	322		
2v = 66.5 mm	Mark.	0.5	6230	484	322	8.9	15.3
	2	5	26950	451	300		
	Mark.	0.5	2890	451	300	10.9	16.5
	3	5	17100	431	288		
	Mark.	0.5	3790	431	288	12.3	17.5
	4	5	20790	418	278		
	Mark.	0.5	2140	418	278	14.1	19.0
	5	5	13720	399	266		
	-	-	-	-	-	15.8	20.5
Tensile specimen 3	0	-	-	-	-	5.6	12.7
w = 33.9 mm	1	5	58000	531	354		
2v = 68.0 mm	Mark.	0.5	4300	531	354	8.8	13.7
	2	5	24000	501	334		
	Mark.	0.5	2700	501	334	10.2	14.8
	3	5	23600	479	320		
	Mark.	0.5	1700	479	320	12.1	15.9
	4	5	14000	460	306		
	Mark.	0.5	2500	460	306	13.3	17.1
	5	5	24750	440	292		
	Mark.	0.5	2100	440	292	15.9	19.5
	6	5	10000	413	276		
	-	-	-	-	-	17.0	21.0

considerably less. The a and c values were corrected for the plastic zone at the crack front by multiplication with M_p^2. Cf. Table 6.

The mathematical a and c values were used for ΔK-evaluations at the end of the axis of the elliptic defect. This was used to achieve convenient and rather equal defect growth in subsequent steps of varying load by keeping the ΔK's at the minor-axis end in the steps equal. Corresponding α and γ values as observed were compared with the (α,γ)-values for which γ was theoretically predicted from a realized α, both according to the Paris relation and the maximum compliance increase hypothesis as describing the 2d-defect growth.
The (α,γ)-values after performance of all loading cycles $\Delta N = \Sigma \Delta N_i \simeq 10^5$ were calculated according to the Paris relation (using the data of Bristoll and Opdam loc.cit). This appeared to offer an underestimate of the observed behaviour (Cf. Fig. 15).
In our opinion, when applying $dc/dN = k(\Delta K)^m$, the "constant" k will now depend on (the ratio of) a and c. Cf. Fig. 16. Using the "maximum compliance increase" hypothesis for defect growth implying $dc/dN = \kappa(\Delta K)^2$ or rather $\kappa(\Delta K)^2\Lambda$, allows to plot $\kappa\Lambda$ vs α/γ (cf. Fig. 16) offering a way to describe the 2d-defect extension with number of load cycles.
For these calculations the following rationale was used:
If α_i and γ_i are the α and γ-values at the end of the i-step, corresponding with ΔN_i load cycles and a $\Delta K_i = \Delta K$, one defines:

$$\bar{\alpha}_i = (\alpha_{i-1} + \alpha_i)/2 \text{ and } \bar{\gamma}_i = (\gamma_{i-1} + \gamma_i)/2.$$

These $\bar{\alpha}_i$ and $\bar{\gamma}_i$ were related to $\Delta K_i = \Delta K$ during step i, by

$$\frac{\Delta \bar{\alpha}_i}{\Delta N_i} = k(\Delta K)^m \text{ and } \kappa(\Delta K)^2\Lambda$$

with m = 2.71 and $k = 1.48 \times 10^{-12}$ (units: MPa and m) for a Paris relation-like description and with m = 2, allowing to evaluate $\kappa\Lambda = \kappa\lambda(\bar{\alpha}/\bar{\gamma})$ for a "maximum compliance increase" description of the 2d-defect extension respectively.
From Fig. 15 it was concluded that the maximum compliance increase description shows a somewhat better agreement than the Paris relation with the experimentally observed 2d-defect extension data.

Compliance and Strain Measurements

According to (18) the compliance and strain would show a linear dependence on $\alpha^{1.7}\gamma^{1.8}$; Fig. 17 shows the verifying plot.
As presumably $C^* = C_o^* + C_o^* \lambda^* \alpha^{1.7}\gamma^{1.8}$ the C_o^*-values can be found as the part cut-off from the C^*-axis, at the same time allowing to find E, as $C_o^* = L/Evw$, while from the slope and the determined C_o^*-value can be concluded to the λ_o^*-value. It was found for tensile specimen 1,2,3 respectively, that E = 208, 201, 204 GPa, thus $\Delta E/E < 2\%$; C_o^* = 0.219, 0.234, 0.223 nm/N; λ_o^* = 0.57, 0.67, 0.63, thus $\Delta\lambda_o^*/\lambda_o^* = 8\%$.
The discrepancy with the numerically evaluated λ_o^*-value of 0.78 in (18) might be due to the experimentally not realized boundary condition as assumed at the f.e.m calculations.

The observed ε-values have to match the calculated values of ε for a stress of 200 MPa by suitable correction for the stress in Table 6. Figure 18 allows this comparison, which proved satisfactory. (The strongly deviating data points of specimen 3 in Fig. 18 are readily explained by a loosening of relevant strain gauges during step 5 and 6 of these measurements, probably the attachment was

TABLE 6a α and γ-values for plastic zone corrected axes dimensions of semi-elliptic surface defect in tensile specimens and corresponding ΔK_a and ΔK_c values.

Specimen	Step nr.	$\Delta\sigma$ (MPa)	a^* (mm)	c^* (mm)	α	γ	$\Delta K_{a\ \frac{1}{2}}$ (MPam$^{\frac{1}{2}}$)	$\Delta K_{c\ \frac{1}{2}}$ (MPam$^{\frac{1}{2}}$)
1	1	156	8.27	12.70	0.243	0.374	20.4	16.4
	2	140	10.07	13.70	0.296	0.403	19.2	16.5
	3	134	11.48	14.70	0.338	0.432	19.1	16.9
	4	134	13.59	16.61	0.400	0.489	20.3	18.4
	5	129	15.19	18.11	0.447	0.533	20.4	18.7
2	1	144	8.97	15.42	0.267	0.459	20.5	15.6
	2	134	10.97	16.61	0.327	0.494	20.2	16.4
	3	129	12.38	17.61	0.368	0.524	20.0	16.8
	4	125	14.18	19.11	0.422	0.569	20.3	17.5
	5	119	15.89	20.62	0.473	0.614	20.2	17.7
3	1	154	8.87	13.81	0.262	0.407	20.9	16.7
	2	145	10.28	14.91	0.303	0.440	20.6	17.2
	3	138	12.18	16.00	0.359	0.472	20.6	18.0
	4	133	13.39	17.21	0.395	0.508	20.6	18.2
	5	127	16.00	19.62	0.472	0.579	21.0	19.0
	6	120	17.10	21.10	0.504	0.623	20.6	18.5

TABLE 6b Comparison of γ as measured with as predicted according to Paris relation and maximum compliance increase hypothesis, respectively.

Specimen	Step nr.	α	γ		
			measured	Paris relat. m = 2.71	max. compliance increase
1	1	0.243	0.374	0.374	0.374
	2	0.296	0.403	0.406	0.412
	3	0.338	0.432	0.435	0.445
	4	0.400	0.489	0.481	0.497
	5	0.447	0.533	0.519	0.538
2	1	0.267	0.459	0.459	0.459
	2	0.327	0.494	0.491	0.498
	3	0.368	0.524	0.516	0.528
	4	0.422	0.569	0.552	0.569
	5	0.473	0.614	0.588	0.610
3	1	0.262	0.407	0.407	0.407
	2	0.303	0.440	0.431	0.436
	3	0.359	0.472	0.468	0.479
	4	0.395	0.508	0.494	0.508
	5	0.472	0.579	0.554	0.573
	6	0.504	0.623	0.580	0.602

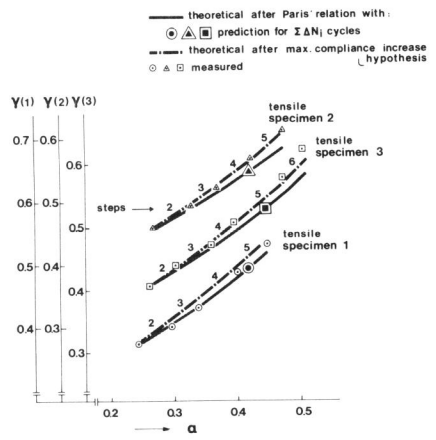

Fig. 15. Comparison of crack shape developments predicted after Paris relation and maximum compliance hypothesis with observed data. Discrepancy for Paris relation prediction with respect to total number of applied cycles and shape development.

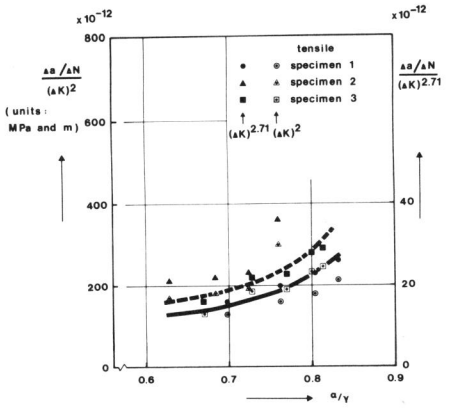

Fig. 16. $k=(\Delta\bar{a}_i/\Delta N_i)/(\Delta K)^{2.71}$ and $K\Lambda=(\Delta\bar{a}_i/\Delta N_i)/(\Delta K)^2$ as function of α/γ for surface defect extension in tensile specimen.

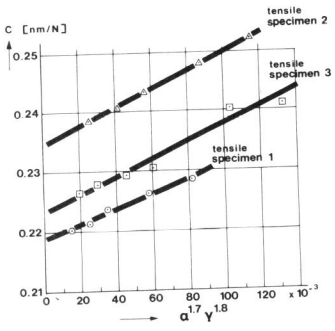

Fig. 17. Compliance C versus $\alpha^{1.7}\,\gamma^{1.8}$ for tensile specimens with surface defect.

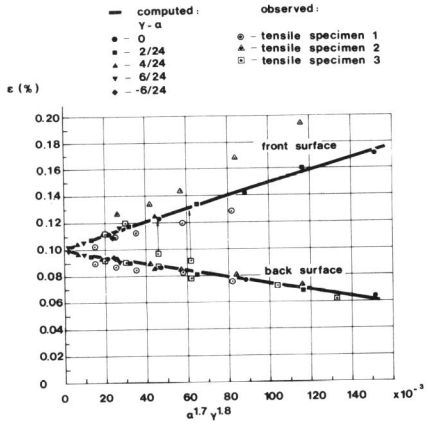

Fig. 18. Computed and observed strains (ε) versus $\alpha^{1.7}\,\gamma^{1.8}$ for tensile specimens with surface defects. ε at x = 27.5 mm; y = 0 mm; z = 2.5 mm; and at x = 27.5 mm; y = 35 mm; z = 2.5 mm.

already poor during step 3 and 4). Strain measurements thus can give some indication of defect growth, be it in this case of $\alpha^{1.7}\gamma^{1.8}$ and not of α and γ separately.

CONCLUSIONS

From related work

It was tried to use the results of other investigators of 2-dimensional defect growth for the present analysis as well. From the measurements of Tenge and Solli (1973) only shape development data could be deduced from tests on specimens submitted to a combination of tensile and bend loading. These do not allow a direct comparison with (18). Aamodt, Bergan and Klem (1973) used the same results as Tenge and Solli.
Aamodt and Bergan (1974 and 1975) graphically presented the results of shape development measurements on surface defects. These could be used near the start and near the end of defect growth. The best n-value for a description $\gamma^n = \gamma_o^n + \alpha^n$ was calculated as 1.15. (According to the Paris relation $n > 2$, according to maximum compliance increase hypothesis to describe the defect growth $n \approx 2$).
Among the measurements of Aamodt en Klem (1977) was one performed in absence of bending. Only 2 combinations (α,γ) were given, with α slightly above 0.5 and $\alpha = 1.0$ respectively, i.e. measurement was performed till complete plate penetration; the material was an Al-alloy and not steel. In view of this, comparison with both discussed defect growth descriptions was not carried out.
Cruse, Meyer and Wilson (1977) communicated on results of extension measurements on a surface defect in a titanium alloy. Two α-values were below 0.5. There was good agreement with the maximum compliance increase hypothesis and somewhat less with the Paris relation for defect extension description.
Collipriest (1972) gave results of extension measurements on a surface defect in a 12 mm thickness Al-alloy plate. From his relevant plot two (α,γ)-combinations were read, offering $n = 2.82$ (which would favour the Paris relation description, though being even for this one too high).
From the work of Hodulak, Kordisch, Kunzelmann and Sommer (1978, 1979) no conclusive arguments favouring one of the here considered descriptions for defect growth were found; these authors assumed an anisotropic fracture resistance and a redistribution of stresses due to plastic strains to explain the experimentally observed deviations of Paris relation-like descriptions for surface defect growth.
Three of the four possible comparisons with literature were in favour of the maximum compliance increase hypothesis, one in favour of the Paris relation, to describe defect growth. In one case the agreement with the maximum compliance increase hypothesis was excellent.

Summarized from here performed work

1. The hypothesis that 2d-defect growth will occur in such a way that a maximum compliance increase is achieved, was confirmed.
2. As shape development relation was suggested: $\gamma^2 = \gamma_o^2 + \mu\alpha^2$ with
   $\mu = 1$ for embedded cracks and
   $\mu = 1.12$ for surface defects
   (rather then $\gamma^n = \gamma_o^n + \alpha^n$ deduceable from the Paris relation).
3. Application of the relation of Paris on surface cracks with constants obtained from through cracks might lead to an underestimate of the surface crack growth rate (cf. Fig. 15).
4. **The description of the normalised compliance for embedded and surface elliptic defects is: $\Gamma = 1 + \lambda\alpha^{3/2}\gamma^{3/2}$ and $\Gamma^* = 1 + \lambda_o^*\alpha^p\gamma^q\alpha^{3/2}\gamma^{3/2}$, respectively ($p = 0.165$; $q = 0.36$; λ and λ_o^* are geometry dependent).**

ACKNOWLEDGEMENTS

This investigation was sponsored by the Dutch Industrial Council for Oceanology instituted by the Ministery of Economic Affairs, as part of the Marine Technology Research Program in the Netherlands. The f.e.m. calculations were carried out by the TNO Software Engineering Section under Mr. F.P. Tolman with his co-workers Mr. M.A. Kusters and Miss A. IJsseldijk of the TNO Department of Structures and Materials, while Mr. A. van Baalen en Mr. C.C.J. Kaasschieter assited at the experiments.

REFERENCES

Aamodt, B. and Bergan, P.G. (1974). Propagation of elliptical surface cracks and non linear fracture mechanics by the finite element method. Proc. of the 5th Conf. on Dimensioning and Strength Calculation, Budapest, Hungary, I-31 - I-42.

Aamodt, B. and Bergan, P.G. (1975). Numerical techniques in linear and non linear fracture mechanics. Proc. of the 2nd Nat. Congr. on Pressure Vessels and Piping, 199.

Aamodt, B. and Bergan, P.G. and Klem, H.F. (1973). Calculation of stress intensity factors and fatigue crack propagation of semi-elliptical part-through surface cracks. Proc. of the 2nd Int. Pressure Vessel Conf. - San Antonio-Texas-USA, 911

Aamodt, B., and Klem, H.F. (1977). Application of numerical techniques in practical fracture mechanics. In: Fracture Mechanics in Engineering Practice. Dept. of Mech. Eng. Univ. of Nottingham, 33.

Bristoll, P.and Opdam, J.J.G, (1975). Fatigue of off-shore structures. The prediction of fatigue crack propagation under conditions of random load. Proc. of Int. Conf. on Oceanology, 3.

Collipriest, J.E. (1972). An experimentalist's view of the surface flaw problem. In: The Surface Crack, ASME, (J. Swedlov, ed.) 43.

Cruse, T.A., Meyers, G.J. and Wilson, R. (1977). Fatigue growth of surface cracks. In: Flow growth and fracture. ASTM-STP, 631.

Forman, R.G., Kearney, V.E. and Engle, R.M. (1967). Numerical analysis of crack propagation in cyclic loaded structures. ASME-Trans. J. Basic. Eng. 89D. 459

Hodulak, L., Kordisch, H., Kunzelmann, S. and Sommer, E. (1978). Influence of the load level on the development of part-through cracks. Int. J. of Fracture, 14. 35.

Hodulak, L., Kordisch, H., Kunzelmann, S. and Sommer, E. (1979). Growth of part-through cracks. ASTM-STP 677. (C.W. Smith, ed.).

Irwin, G.R. (1960). Plastic zone near a crack and fracture toughness. Proc. 7th Sagamore Conf., p. IV-63.

Irwin, G.R. (1962). The crack extension force for a part-through crack in a plate Trans ASME, J. Appl. Mech., 651.

Kobayashi, A.S. and Moss, W.L. (1969). Stress intensity magnification factors for surface flawed tension plate and notched round tension bar. Proc. 2nd. Conf. on Fracture. Brighton - U.K. (Chapmann & Hall Ltd.), 31.

Overbeeke, J.L. (1978). Progress Report on the European Community - Collaborative Program on fatigue and corrosion fatigue behaviour of off-shore steel structures, ECSC-contract No 7210-KB/6/602. Mech. Eng. Laboratory, Techn. Univ. Eindhoven, The Netherlands.

Paris, P.C. (1962). The growth of fatigue cracks due to variations in load. Thesis Lehigh University.

Paris, P.C., Gomez, M.P. and Anderson, W.E. (1961). A rational analytic theory of fatigue. The Trend in Engineering, 13, 9.

Pelloux, R.M.N. (1970). Review of theories and laws of fatigue crack propagation. Air Force Conf. on Fatigue and Fracture AFFDL-TR-70-144, 409.

Saxena, A., Hudak, S.J., and Jouris, G.M. (1979). A three component model for representing wide range fatigue crack growth data. Eng. Fr. Mech. 12, 103.

Tenge, P, and Solli, O. (1973). Fracture Mechanics in the design of large spherical tanks for ship transport of L.N.G., 1.